This is the submitted version of the paper https://doi.org/10.1039/D1SE00030F
published in Sustainable Energy & Fuels on February 18th, 2021

Journal Name

ARTICLE TYPE

Cite this: DOI: 00.0000/xxxxxxxxxx

Palliating the efficiency loss due to shunting in perovskite/silicon tandem solar cells through modifying the resistive properties of the recombination junction†

Claire Blaga[a], Gabriel Christmann[a], Mathieu Boccard[b], Christophe Ballif[ab], Sylvain Nicolay[a] and Brett A. Kamino*[a]

Received Date
Accepted Date

DOI: 00.0000/xxxxxxxxxx

As the efficiency of commercial crystalline silicon solar cells approaches its maximum theoretical value, tandem architectures are becoming increasingly popular to continue the push to higher photovoltaic performances. Thin-film materials are particularly interesting partners for silicon wafers due to their potential cost effectiveness and ease of fabrication. However, in large scale thin-film coatings, particularly for perovskite materials, avoiding the formation of point shunts is a challenge. This study investigates the sensitivity of perovskite/silicon tandems to such shunts and whether or not optimising the lateral and transverse resistances of the recombination junction can reduce the negative effects of these defects. To do so, the inhomogeneous characteristic of shunts is reproduced by modelling tandem cells with an array of scaled equivalent circuit elements connected in parallel. It is shown that by optimising the resistive properties of the interconnection, there can be a an important quenching effect on shunts present in the top cell, resulting in a significant increase in the overall cell efficiency at STC and at low light conditions. These findings give a clear pathway on how to bridge the efficiency gap between small laboratory cells, which can be selected shunt free, and industry scale devices, which are more prone to localised shunting.

1 Introduction

The development of low cost, high efficiency photovoltaic (PV) devices is becoming increasingly important as society moves towards replacing fossil fuels by sustainable energy sources. Currently, the most common solar cells on the market are crystalline silicon (c-Si) single junction devices which have reached a record efficiency of 26.7% in the case of silicon heterojunctions with intrinsic thin layer (HIT).[1] However, silicon-based photovoltaic devices are slowly approaching their Shockley-Queisser limit (32% for c-Si[2]) and more importantly, their maximum theoretical efficiency, evaluated at 29.5%.[3] Nonetheless, silicon (Si) based PV are projected to continue dominating the market.[4] Furthermore, as the balance of PV sytems (BOS) costs become the driving factor, it is important to increase the efficiency of modules in order to increase the electricity yield per unit area and reduce the levelised cost of electricity (LCOE) of installations.[5]

As efficiency limits are obtained by factoring in sub-bandgap and thermalisation losses,[6] one practical solution to continue the growth of solar cell efficiencies is therefore to reduce these spectral losses through a tandem architecture. By stacking two single junctions monolithically (2-terminal) or mechanically (4-terminal), the power conversion efficiency (PCE) reaches a theoretical limit of about 42% - 45%.[7,8,9]

Potential partner sub-cells for silicon wafers in multi-junction PV devices are hybrid organic-inorganic metal-halide perovskite solar cells (PSCs). This thin-film technology is undergoing considerable research due to its advantageous optoelectronic properties including strong solar absorption, steep absorption edge[10] and low non-radiative carrier recombination rates, making perovskite a promising active material for solar cells[11]. Furthermore, the high tolerance to defects[12,13] and low temperature solution processability compared to other thin film materials enables a low-cost and easy fabrication process that is compatible with various other materials.[14] Their tunable bandgaps also allow PSCs to be adapted for tandem applications.[15]

These properties make perovskite materials an excellent match for silicon in a tandem architecture. At present, the record efficiency for monolithic perovskite/silicon tandems has been achieved by the Helmholtz Zentrum Berlin with 29.15%[16] but there is still significant potential to push the efficiency closer to a practical limit of 38%.[17]

[a] PV-Center, CSEM, Rue Jaquet Droz 1, 2002, Neuchatel, Switzerland.
[b] Institute of Microengineering (IMT) Photovoltaics and Thin-Film Electronics Laboratory (PV-Lab), Ecole Polytechnique Federale de Lausanne (EPFL), Rue de la Maladiere 71b, 2002, Neuchatel, Switzerland.

† Electronic Supplementary Information (ESI) available. See DOI: 00.0000/00000000.

One factor hindering the developments of such high efficiency cells is the limitations of the processing control when fabricating perovskite films, mainly in terms of their homogeneity.[18,19] This can lead to small electronic defects called shunts, in which the resistance between the cell's two contacts is greatly reduced. This is especially the case for large area film coating for which thin film continuity is difficult to achieve, especially on substrates with some degrees of roughness.[20] Therefore, understanding the impact of these defects will play an important role in the scaling up of perovskite/silicon tandems. However, this is not straightforward in tandem devices as the effect of shunts on the light-IV (LIV) characteristics is complex and varies significantly from their effects on single junction devices.[21] Eventually, the extent of the damage to the cell performance depends on the severity of the shunt but also on other factors which can have mitigating effects.

One particular element that could mitigate the performance loss due to shunts is the resistive properties of the recombination junction (RJ), which connects the two sub-cells of a monolithic tandem solar cell in series. This approach is well known from another monolithic tandem technology based on amorphous silicon and microcrystalline silicon subcells (micromorph). Despeisse *et al.* have reported that for these micromorph solar cells grown on substrates with high light trapping potential, adding a resistive, doped nano-crystalline silicon oxide interlayer at the recombination junction can reduce the impact of local current drains created during deposition due to the highly textured surface.[22] Additionally, Rau *et al.* found that the degradation of the cell performance due to spatial variations of the electronic properties can be limited by increasing the local series resistance imposed on the electrons travelling from the inhomogeneous region to the contact.[23] However, there are still some limitations in the understanding of this approach, especially concerning its analysis through modelling.

Solar cells in the dark are essentially diodes formed by a p-n junction. When illuminated, the diode characteristic is offset by the photogenerated current, which behaves as an ideal current source. Solar devices can thus be modelled by an equivalent electrical circuit composed of one or more diodes as well as elements representing the generation and losses occurring in the cells when they are illuminated. This has previously been done to examine various aspects of single or multi-junction solar cells. These models include simple circuits, consisting of either one subcircuit (composed of one or two diodes, a current source, a parallel and a series resistance) for single junctions, or two connected in series for tandems, forming what is here on referred to as a single element.[24,25] There are also more complex models with many single elements connected in parallel, allowing to model the cell's inhomogeneity.[21,23] This type of circuit can therefore be used to simulate a point shunt within the planar geometry of a cell.

This study aims to understand the effect of shunts on the electronic behaviour of perovskite/silicon tandem solar cells. Using a circuit array model with many single elements connected in parallel, the approach of Despeisse *et al.* will be adapted to perovskite based tandems; the influence of the lateral and transverse resistances of the recombination junction on the performance of devices with small shunt defects will be analysed in order to determine if and under which conditions it is possible to mitigate the negative effect of such defects.

2 Experimental

2.1 Modelling solar cells

Solar cells, in the dark and under ideal conditions, behave according to the Shockley diode equation.[26] In reality, these devices do not follow the ideality criteria, mainly due to the presence of non-radiative recombination mechanisms. Nonetheless, their behaviour can still be approximated by the modified diode equation (1).

$$I = I_{ph} - I_s \left[\exp\left(\frac{q(V+IR_s)}{Ak_BT} \right) - 1 \right] - \frac{V+IR_s}{R_{sh}} \qquad (1)$$

The latter includes the photocurrent, I_{ph} produced by photogenerated carriers when the cell is illuminated. It also accounts for shorts caused by defects in the cell such as pin holes or grain boundaries with the parallel resistance, R_{sh}, and for the contact resistance between the semiconductor and the contacts as well as the bulk resistances with the series resistance, R_s. Furthermore, the recombination mechanisms other than the band-to-band radiative process supposed in the ideal Shockley equation are modelled by the ideality factor, A, as well as a larger value of the diode saturation current, I_s. In the one-diode model, A is an average of the ideality factors of the different recombination processes occuring in the cell. Models with additional diodes also exist, which allow to account for the separate mechanisms by assigning an ideality factor corresponding to a particular recombination process to each diode.

Equation (1) is a simple model for a single junction. In order to obtain the required complex equivalent circuit model of a tandem solar cell, the approach to follow is outlined by the flowchart of Figure 1. Input data of this model are the experimental LIV curves of real silicon and perovskite single junctions as well as of a perovskite/silicon tandem. The fabrication of these solar cells is detailed in the following section.

2.2 Solar cell fabrication

Single junction perovskite solar cells were fabricated on commercial 7 Ω/□ ITO substrates which were cleaned using standard methods. A 20 nm p-contact was formed by RF sputtering of nickel oxide under a pure argon gas flow which was then annealed at 300 °C for 15 minutes in air. After annealing, the substrates were cooled and immediately placed in an inert atmosphere glovebox where the perovskite layer was deposited by spin coating using an anti-solvent quenching method. The perovskite layer had a nominal composition of $Cs_{0.17}FA_{0.83}PbI_{0.83}Br_{0.17}$ which was quenched using chlorobenzene. The perovskite layer was annealed at 120 °C for 30 minutes followed by deposition of the n-type stack by thermal evaporation. This stack was composed of LiF (1 nm) followed by C_{60} (15 nm) and finally completed with a Ag (100 nm) electrode.

Single junction silicon heterojunction cells were fabricated using 4-inch, n-type, float zone wafers with a <100> orientation and mechanically polished front surfaces. To perform rear side texturing of the wafers, the front sides were protected by a 200 nm thick SiNx coating deposited by PECVD. Then the rear side of

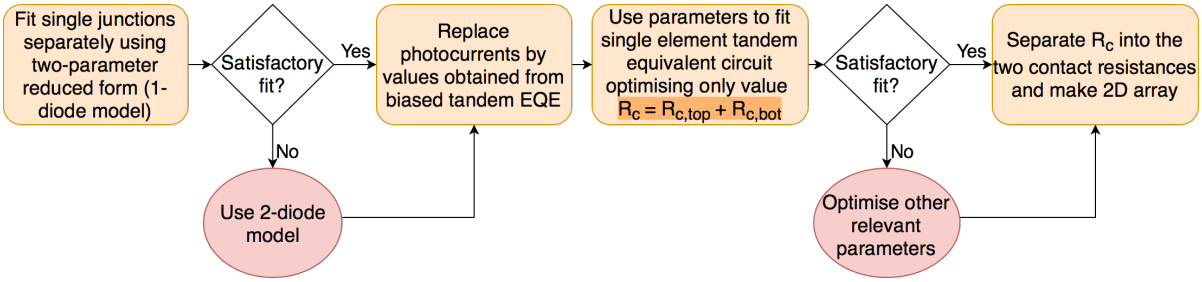

Fig. 1 Steps followed to fit the equivalent circuit model parameters to the experimental tandem LIV characteristic

the wafers was textured using a standard KOH etch followed by removal of the SiNx in a HF bath. Standard cleaning was then performed and, after a brief HF treatment to remove the native oxide, the wafers were coated with thin amorphous silicon layers using a PECVD tool. On the rear side, a stack of intrinsic amorphous silicon then p-type amorphous silicon was deposited. Similarly, the front side was passivated using a stack of intrinsic amorphous silicon followed by n-type amorphous silicon. These cells were completed by depositing a patterned layer of ITO/Ag onto the rear side and an ITO layer on the front side. The cells were finally finished by printing a metal grid onto the front surface.

The tandem solar cell stack upon which the model in this study is based is shown in Figure 2. The cell diagram is shown in supplementary information SP1. These cells were fabricated using silicon heterojunction bottom cells as described above. However, a 10 nm ITO layer was deposited as the recombination junction, followed by 20 nm of NiO as above. These wafers were annealed at 200 °C for 10 minutes prior to the deposition of the perovskite and n-type stack as described above. On top of the C_{60} layer, 10 nm of SnO_2 was grown using an ALD tool at 120 °C. To form the front contact, 65 nm of tungsten doped indium oxide was deposited by RF sputtering, followed by 100 nm of thermally evaporated Ag in a grid pattern. Finally, a 100 nm film of MgF_2 was thermally evaporated to form an anti-reflective layer.

2.3 Characterisation

LIV measurements were made on a AAA solar simulator with two light sources (xenon and halogen). The solar simulator was calibrated for both intensity and spectral response by using a set of externally calibrated reference cells with various filters. Cells were held on a metallic chuck that was thermally regulated to 25 °C and contact was made using Kelvin probes. All cells were illuminated through opaque illumination masks with known areas. Cells with perovskite layers were scanned at a rate of approximately 80 mV/s and maximum power point tracking was performed using a 3-point algorithm to approximate a steady-state output of the cells. External quantum efficiency (EQE) measurements were made using a home-built setup which was calibrated using a certified reference cell. For tandem measurements, blue and red light biases were used to isolate the spectral response from each sub-cell. Additionally, an electronic DC bias of +0.6 V was applied to the tandem when measuring the top perovskite cell to ensure that it was being measured near short-circuit current.

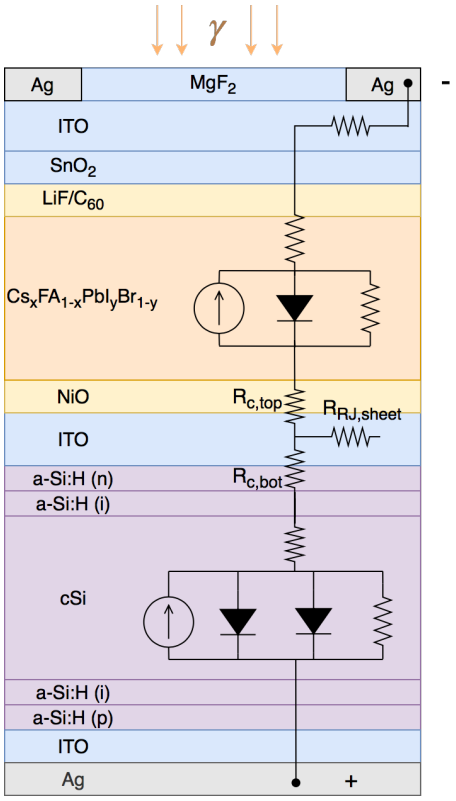

Fig. 2 Modelled cell stack of the perovskite/silicon tandem solar cell with superimposed equivalent circuit of a single element

2.4 Equivalent circuit model

The parameters of a single element of the tandem solar cell's equivalent circuit (Figure 2) are obtained by first separately fitting the LIV curves of the sub-cells to the diode equation (1) (see supplementary information SP2 and SP3). The silicon heterojunction cell is fitted to a two-diode model as the sharp knee of the former's LIV curve indicates a change in the dominating recombination process with the injection level. These different mechanisms are thus accounted for by two different diodes whose ideality fac-

tors are set to $A_{1,bot} = 1$ and $A_{2,bot} = 2$. The parameters extracted from this are then used to fit the tandem's LIV curve. However, the photocurrents found for the single junctions are first changed to the values obtained from the experimental biased EQE of the tandem solar cell (Figure 3 (left)). Based on these values, the fit of the perovskite/silicon tandem LIV shown in Figure 3 (right) is obtained by using a Simulation Program with Integrated Circuit Emphasis (SPICE) and modifying the remaining unknown parameters.

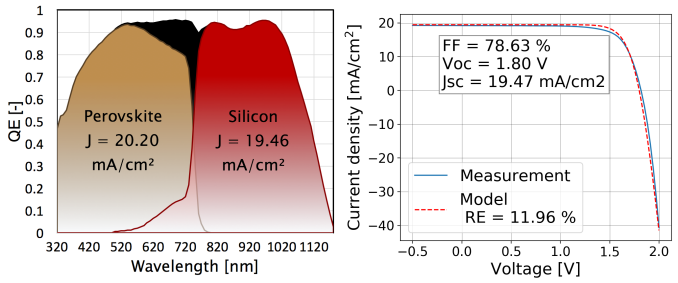

Fig. 3 Left: Tandem solar cell EQE; the shaded areas correspond to the photocurrent contributions of the subcells (integrated over an AM1.5G spectrum) and the black curve represents the sum of the photocurrents. The short circuit currents extracted from this measurement are 20.20 mA/cm^2 for the perovskite sub-cell and 19.46 mA/cm^2 for the silicon sub-cell. Right: Fitted experimental LIV curve of the perovskite/silicon tandem solar cell.

The parameters of the equivalent circuit extracted from this tandem fit are shown in Table 1. These are used to create the 2D array circuit and unless stated otherwise, are the baseline parameters used in the simulations. The 2D circuit is composed of single elements connected in parallel in a two-dimensional grid by the ITO and recombination junction sheet resistances, $R_{ITO,sheet}$ and $R_{RJ,sheet}$ respectively, as shown in Figure 4. The series resistances of each sub-cell of the single elements are separated into the contact resistances to the RJ, $R_{c,top}$ and $R_{c,bot}$ and generic series resistances, $R_{s,top}$ and $R_{s,bot}$. This is done to single out the contact resistances with the RJ as it is one of the studied elements. The generic series resistances account for all other contact resistances between the layers of each sub-cell as well as the bulk resistances of the absorbers. In this configuration, the values of the circuit elements have to be scaled to the size and number of elements in the array (see supplementary information SP4). In this study, the results are obtained using a 30×30 array of single elements and solving this equivalent circuit using a SPICE. Shunting is introduced by setting the shunt resistance, R_{sh}, of a sub-cell in selected single elements to zero. These elements are selected in a spiral order starting from the single element at the centre of the array. The number of these elements, N, is based on the fraction of the active area that is to be shunted, f, which also depends on the size of the array as follows:

$$N = \lceil f \times m \times n \rceil \tag{2}$$

where m and n are the number of rows and columns of the circuit array.

Although this equivalent circuit is a good approximation of the

Table 1 Unscaled circuit element parameters of the perovskite/silicon tandem solar cell

Parameter	Value
$R_{ITO,sheet}$	55 Ω/□
$R_{s,top}$	1.33 Ωcm^2
$I_{s,top}$	9.4 ×10^{-12}A/cm^2
A_{top}	1.95
$R_{sh,top}$	2250 Ωcm^2
$I_{ph,top}$	20.2 mA/cm^2
$R_{c,top}$	0.5 Ωcm^2
$R_{c,bot}$	0.3 Ωcm^2
$R_{RJ,sheet}$	450 Ω/□
$R_{s,bot}$	0.4 Ωcm^2
$I_{s1,bot}$	8.8×10^{-15}A/cm^2
$I_{s2,bot}$	9.9×10^{-9}A/cm^2
$A_{1,bot}$	1
$A_{2,bot}$	2
$R_{sh,bot}$	100 kΩcm^2
$I_{ph,bot}$	0.0325 A/cm^2

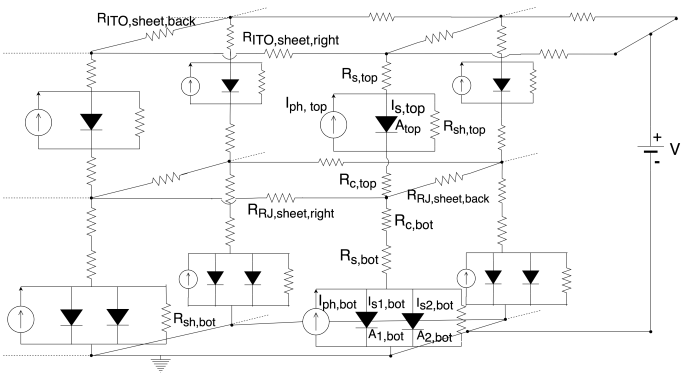

Fig. 4 Scheme of a 2D array equivalent circuit model of a tandem solar cell (example of a 2 × 2 array)

workings of a solar cell, there are a few limitations to this model. Firstly, unlike perovskite, the silicon absorber has a non-negligible lateral conductivity, which is not modelled in this study. For simplicity, it is therefore established that the resistance, $R_{RJ,sheet}$, accounts for both the silicon and RJ parallel sheet resistances, which is valid as long as the contact resistance between them is not too large. However, this implies that for a rear-junction silicon solar cell, the maximum value of $R_{RJ,sheet}$ is the silicon wafer's sheet resistance, which is approximately 200 Ω/□. Indeed, once the sheet resistance of the RJ becomes larger than that of the silicon wafer, charge carriers will simply pass through the wafer instead of the RJ. Secondly, the cell stacks of the sub-cells in tandem configuration are not the same as those of the single junctions. Notably, the back contact of the perovskite single junction is highly crystalline and conductive ITO as the measurements of the cell rely on the lateral conductivity of this layer. In tandem configuration, transport through the ITO RJ is not relied upon to collect current and so this ITO is more resistive. In this case, the device configurations present different systematic series resistance sources that are not inherent to the device stack. Another limiting factor is that the RJ contact resistances are obtained from fitting the tandem's LIV. This could give inexact values due to fitting errors. However, no direct measurement has been done as this is not straightforward and outside of the scope of this article. Finally, the shunt mod-

elled in this study is one within the absorber. For a different type of shunting, for example from the metal contact to the ITO recombination junction, the relation between the circuit elements' effects on the cell performance in presence of a shunt would be different. In particular, it would change the dependence between the sheet resistance and the shunted junction's series resistance, which will be discussed later.

3 Results & discussion

Using the previously constructed equivalent circuit model, the effect of varying the recombination junction's contact and sheet resistances will be investigated based on previous reports for micromorph cells. This will allow to determine if optimising these properties can result in an improved resilience to shunts in perovskite/silicon tandem solar cells.

3.1 Recombination junction resistance

3.1.1 Top shunted tandem

When defects are present in perovskite/silicon tandem solar cells, it is often the top cell that is defective. This is simulated by introducing a shunt in the perovskite sub-cell representing 0.4% of the cell area. This leads to a reduced V_{oc} and an increase in the slope of the LIV curve near the maximum power point (MPP) resulting in a decrease of the cell's FF and PCE (see Figure 5 (left)).

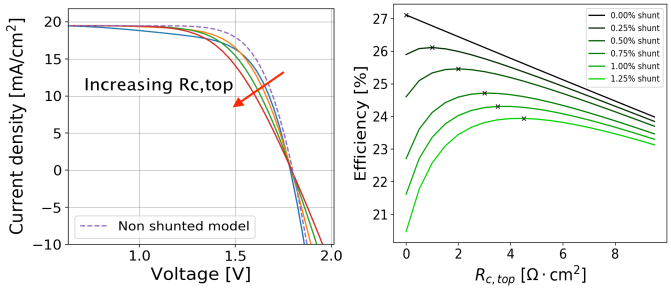

Fig. 5 Left: IV curves of a 0.4% top shunted cell for increasing contact resistances between the RJ and the top cell $R_{c,top}$. Right: Efficiency of a top shunted cell when varying the contact resistance between the RJ and the top cell $R_{c,top}$. The maximum efficiency is marked by an 'x'. For both graphs, the RJ's sheet resistance is maintained at its baseline value of $R_{RJ,sheet} = 450\Omega/\square$

To palliate this effect, an increase in the contact resistance between the perovskite sub-cell and the RJ is considered, based on previous experiments by Despeisse *et al.* on micromorph cells. This is done by modifying the value of the resistance $R_{c,top}$ in the circuit equivalent model (Figures 2 and 4).

When increasing the RJ contact resistance between 0 and 9 $\Omega{\cdot}cm^2$, Figure 5 (left) shows that, while the values of the V_{oc} and I_{sc} are only marginally increased from their initial respective values of $V_{oc} = 1.786$ V and $J_{sc} = 19.46$ mA/cm^2 at $R_{c,top} = 0\ \Omega{\cdot}cm^2$, the slopes of the LIV curve at both the V_{oc} point (R_{oc}) and near the MPP on the J_{sc} side are decreased. These have opposing effects; the first decreases the FF by increasing the effective series resistance of the tandem while the other restores the loss in FF caused by the presence of a shunt. There is therefore a maximum efficiency for shunted cells which can be attained by optimising the value of the contact resistance. For a 0.4% shunted cell, this amounts to an absolute increase in efficiency of 0.36% between the baseline and optimised contact resistance values. This represents a significant increase which is all the more important if the shunt is of higher severity.

This gain in efficiency with optimised contact resistance to the RJ can be explained by a decrease in the current leakage through the shunt due to the increased resistance of the path from the absorber to the RJ. This means that fewer charge carriers will travel through the shunt to recombine in the RJ instead of being extracted at the contacts (see supplementary information SP5). This quenching of current leaks is evidenced by a gain in efficiency which increases with the shunt fraction as shown in Figure 6. Nonetheless, the effect is countered by the losses relative to the additional series resistance induced by $R_{c,top}$. The emergence of an optimal contact resistance between the shunted sub-cell and the RJ is in accordance with the experimental observations found by Despeisse *et al.*.

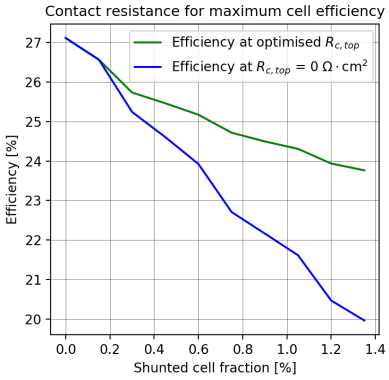

Fig. 6 PCE as a function of the shunted cell fraction for top shunted tandems in cell centre with no contact resistance to the RJ (blue) and with the optimised value of the contact resistance $R_{c,top}$ (green)

In addition, it is observed that the value of $R_{c,top}$ which results in the highest efficiency changes with the shunt fraction as shown in Figure 5 (right). This optimal contact resistance increases with increasing shunt severity since a higher shunt fraction yields a higher leakage current and thus requires a larger resistance to impede its passage.

An analysis of the effect of modifying the lateral resistivity of the oxide interlayer of the cells from its experimental value of $450\Omega/\square$ was also conducted. However, the influence on the cell performance of varying this parameter is much less notable than when changing the contact resistance to the RJ, as shown by Figure 7. Only the slope near the MPP is decreased (Figure 7 (left)) which leads to a negligible increase in the FF and efficiency and no subsequent decrease of the efficiency. Indeed, increasing this resistance does not affect the series resistance of the cell. There can therefore not be a maximal value of the sheet resistance which leads to a performance loss. On the contrary, a high sheet resistance ensures a good isolation between the single elements of the circuit.

The marginal increase in cell performance is due to the high series and contact resistances of the top cell (see Table 1). As

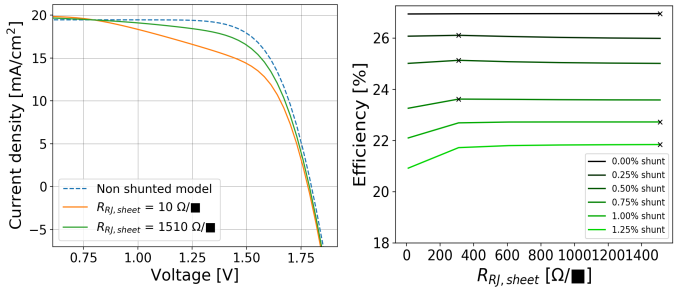

Fig. 7 Left: IV curves of a 0.4% top shunted cell for increasing RJ's sheet resistances $R_{RJ,sheet}$. Right: Efficiency of a top shunted cell when varying the RJ's sheet resistance $R_{RJ,sheet}$. The maximum efficiency is marked by an 'x'. For both graphs, the contact resistance between the top cell and the RJ is maintained at its baseline value of $R_{c,top} = 0.5\Omega{\cdot}\text{cm}^2$

such, the current leak through the shunt is already diminished and few charge carriers travel laterally through the RJ. Increasing the RJ's sheet resistance therefore has a minimal impact on the cell performance.

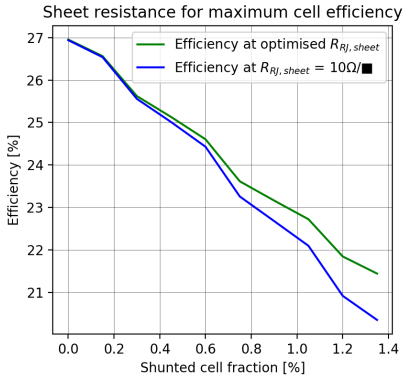

Fig. 8 Efficiency as a function of the shunted cell fraction for a top shunted cells with a low RJ sheet resistance ($R_{RJ,sheet} = 10\Omega/\square$) (blue) and with an optimised RJ sheet resistance (green)

Figure 8 shows that the shunt palliating effect is only significant for high shunted cell fractions when comparing cells with the optimal sheet resistance to ones with a highly conductive RJ ($R_{RJ,sheet}$ = 10 Ω/□). Furthermore, when doing a similar comparison to cells with the RJ's baseline sheet resistance ($R_{RJ,sheet}$ = 450 Ω/□) (see supplementary information SP6), optimising $R_{RJ,sheet}$ has almost no mitigating effect on the loss of efficiency due to shunting. From these results, it is clear that increasing the RJ's sheet resistance from its baseline value has little impact on the cell performance at STC. This is an important fact as the lateral and contact resistances of this layer are not independant; modifying the carrier concentration in the ITO will alter both the sheet resistivity as well as the contact resistance. Thus, this allows to concentrate on optimising the RJ's contact resistance to the shunted sub-cell without needing to worry about the effect of its sheet resistance.

3.1.2 Bottom shunted tandem

Although commercial silicon cells are not typically subject to shunts, it is important to understand the behaviour of shunted tandem solar cells beyond the commercial applications; mild shunting can be used as a proxy for a defective bottom cell which could be caused by a rear scratch or by a front/back interconnection due to bad shadowing during TCO deposition in the HJT. Furthermore, shunting the bottom cell allows to further explore how the approach taken in this study is affected by having subcells with different properties. This is especially applicable to all-perovskite tandems in which shunts are likely to be present in both the top and bottom sub-cells. In these types of tandems, the lateral conductivity of perovskite is negligible, allowing for the equivalent circuit of this study to properly model the effect of the RJ's sheet resistance. In this mindset, a bottom shunted tandem is analysed using the same model and circuit parameters as before.

Figure 9 (left) shows that the behaviour of the efficiency when varying the contact resistance $R_{c,bot}$, between the RJ and the bottom cell (see Figure 2) is similar to the case of a top shunted cell. However, when increasing the sheet resistance of the RJ, the efficiency increase is much more pronounced than it is for a top shunted cell as shown by Figure 9 (right). Indeed, increasing the sheet resistance from 10 to 1500 Ω/□ increases the absolute cell efficiency by over 5% for a 1% shunted bottom cell against an efficiency increase of under 1% for a top shunted cell. This can be attributed to the higher series and RJ contact resistances in the perovskite sub-cell compared to the silicon sub-cell; the former's series resistance is three times larger than the latter's. This means that increasing the RJ's sheet resistance in a top shunted cell will quickly make it unfavourable for charge carriers to travel through the RJ to recombine rather than to travel to the metal contacts and so the efficiency will saturate. But for charge carriers generated in the bottom absorber, the path resistance through the bottom shunt and laterally in the RJ is smaller. Thus, a larger increase in the sheet resistance is needed to impede this passage and a larger efficiency gain can be obtained in doing so.

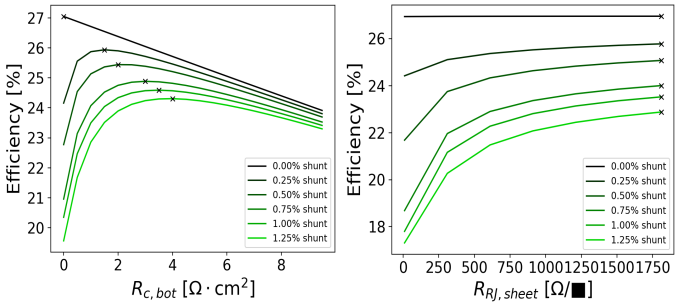

Fig. 9 Efficiency of a bottom shunted tandem cell when varying the contact resistance between the RJ and bottom cell $R_{c,bot}$ (left) and varying the RJ sheet resistance $R_{RJ,sheet}$ (right). The maximum efficiency is marked by an 'x'.

3.2 Design considerations

From the previous observations, some design considerations can be taken for Pk/Si cells with potential shunting in the top cell. Perovskite solar cells appear to have inherently high series resistances compared to other solar cell materials.[27] As previously discussed, this means that the sheet resistance of the recombi-

nation layer has little impact on the cell performance of a top shunted cell. However, a non-zero contact resistance to the recombination junction can considerably increase the cell efficiency. By optimising its value based on the severity of the shunt, the contact resistance can partially palliate the loss in performance by increasing the cell's open circuit voltage. Practically, this could be done by modifying the deposition properties of the ITO layer serving as the recombination junction; by varying the oxygen incorporation as well as other properties of the sputtering deposition process, the carrier concentration can be varied, thus modifying the resistance. Although this would allow to tune the contact resistance, this process will inevitably modify the sheet resistance of the RJ.[28] Nonetheless, based on the previous discussion, this should not affect the cell performance as the efficiency quickly saturates with increasing RJ sheet resistance. Another solution could be to incorporate a graded oxygen content, which would only affect the first few nanometers of the ITO and thus only impact its contact resistance. A preventive contact resistance could therefore be incorporated into the cell design based on the average shunt severity of a given type of thin-film cell. This would allow for a general increase in efficiency of cell batches if these are often subject to a certain level of shunting.

Although the contact resistance to the RJ can be modified to mitigate the effects of shunting, one has to carefully decide whether it is worth focusing on these properties, which are detrimental to non-shunted cells, or whether the focus should be placed on reducing the shunts. For low shunt fractions, the efficiency gained by optimising the contact resistance to the RJ is considerably smaller than that gained by removing the shunt. Therefore, there is a shunt severity threshold after which these solutions could be taken into account in the cell design, but below which reducing shunt defects should be the primary concern. The value of this critical shunt will be determined by the manufacturing process.

3.3 Sensitivity analysis

The previously obtained results are for a perovskite/silicon tandem cell under one sun illumination. However, the goal is for these cells to be commercialised and therefore be used under natural illumination. As the sun travels across the sky, both the intensity of the incident radiation and the current matching of the tandem's sub-cells are affected. Under real conditions, these properties are modified simultaneously as the radiation's spectrum changes with its intensity, but since the dependance between them is complex, they will be changed seperately in the model is order to carry out a sensitivity analysis on the effect of the illumination.

Under one sun illumination, the perovskite/silicon tandem solar cell on which the equivalent circuit model is based is bottom-limited. That is, the photocurrent of the bottom cell is lower than that of the top cell. Since the sub-cells are connected in series, this means that the tandem's overall photocurrent is that of the bottom cell. To look at the effect of the current matching alone, the photocurrents of the sub-cells are modified by changing the values of the current sources in the equivalent circuit as follows:

$$\begin{aligned} I_{ph,top,NEW} &= I_{ph,top} - \delta I \\ I_{ph,bot,NEW} &= I_{ph,bot} + \delta I \end{aligned} \tag{3}$$

This ensures that the sum of the photocurrents of the two sub-cells remains the same.

Figure 10 shows the evolution of the efficiency and fill factor with the top cell current mismatch ($I_{ph,top} - I_{ph,bot}$), for a non-shunted tandem as well as tandems with 0.1% and 0.4% shunted top cells. From this, one can see that for no or low shunting, the fill factor has a minimum at a slightly top-limited condition and has a steeper increase when mismatching towards a bottom-limited condition. As the shunt fraction increases, the minimum disappears and the fill factor keeps decreasing as the cell is mismatched towards increasingly top-limited conditions. Additionally, the fill factor approaches a linear correlation with the top current mismatch. Thus, in most cases, the fill factor is superior in the bottom-limited conditions. This can be attributed to the superior properties of the bottom silicon sub-cell, although ongoing progress is being made on the FF of perovskite cells.

When looking at the cell efficiency as a function of the current mismatch, one can see that it reaches a maximum in bottom-limited conditions as this is where the fill factor is highest. The efficiency peak does not occur at matched photocurrent conditions since it is obtained when the sub-cell currents at maximum power point are matched. When the shunt fraction is increased, the maximum efficiency decreases and moves towards a more bottom-limited condition. This is because a more important top shunt means that more photogenerated carriers from the top cell will travel through the shunt and towards the RJ to recombine. However, having a higher photogeneration rate in the shunted cell means that more current needs to be leaked by the shunt to see negative effects on the cell performance[21] The opposite is true if the shunt is in the bottom cell; the maximum efficiency occurs in top-limited conditions.

The optimal current matching is highly dependant on the cell properties and the shunt severity. For the considered shunted cell fractions, the increase in cell efficiency achieved by optimising the current matching is very small compared to that lost due to the presence of shunt defects. Consequently, optimising the current matching for potential shunting would not significantly increase the cell's performance. During cell conception, the currents should rather be mismatched towards a condition where the cell with the least potential of shunting is limiting.

One can then determine whether the current matching affects the previous observations made when varying the RJ's transverse and lateral resistances. To analyse this, only a top shunted cell is considered as this is the more realistic case. Figure 11 shows that the best performance is always attained when the cell is in bottom limited conditions and the worst in top limited conditions, in concurrence with the previous results. Nonetheless, this represents, in both cases, a loss in absolute efficiency of less than 1%. Varying the RJ's sheet resistance or its contact resistance to a top shunted cell under different illuminations therefore does not cripple the

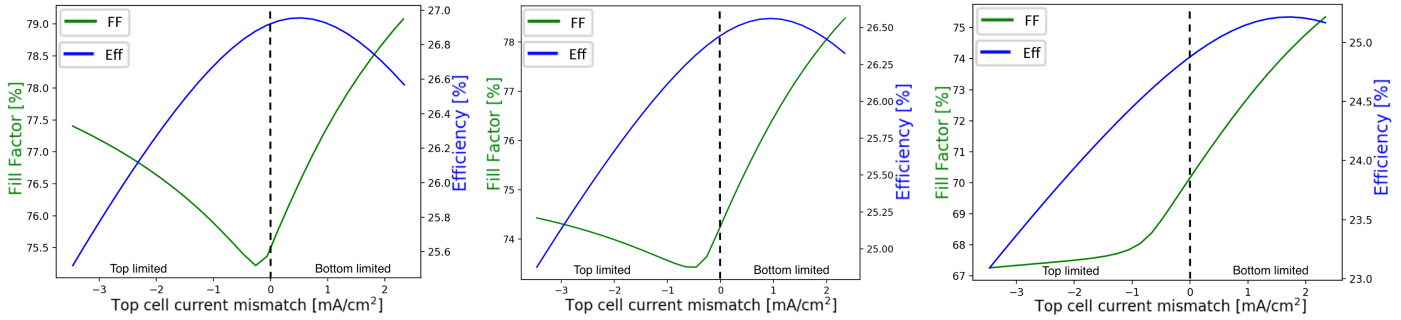

Fig. 10 Fill factor and efficiency of perovskite/silicon tandem solar cells without shunting (left), 0.1% local top shunt (centre) and 0.4% local top shunt (right) as a function of the top current mismatch $I_{ph,top} - I_{ph,bot}$

cell performance. Furthermore, although the efficiency is lower in current matched or top limited conditions, the trend it follows when increasing the contact resistance to the RJ's is the same as in bottom limited conditions. When varying the RJ's sheet resistance, a shunt fraction of 1% is considered in order to have more obvious results. In this case, the same initial increase in efficiency is seen with increasing sheet resistance. However, the efficiencies of the current matched and top limited cells saturate much slower than that of the bottom limited cell.

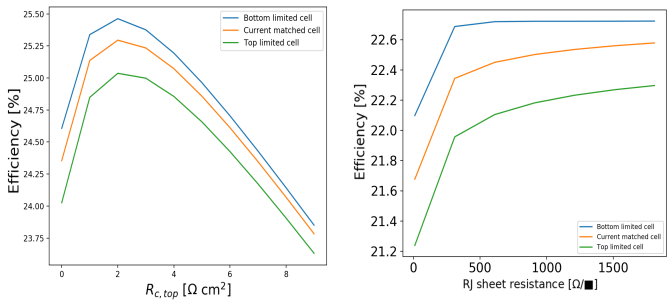

Fig. 11 Comparison of the current matching effect on the efficiency of a 0.4% top shunted perovskite/silicon tandem when varying the top contact resistance to the RJ (left) and a 1% top shunted tandem when varying the RJ sheet resistance (right). Bottom limited: $I_{ph,top} - I_{ph,bot} = 0.74$ mA/cm^2, Current matched: $I_{ph,top} - I_{ph,bot} = 0$ mA/cm^2, Top limited: $I_{ph,top} - I_{ph,bot} = -0.74$ mA/cm^2

To further pursue this sensitivity analysis, the effect of decreasing the light intensity is analysed by reducing the photocurrents of both sub-cells to 10% of their initial values. When increasing the contact resistance to the recombination junction, Figure 12 (left) shows that, for the same range of values of $R_{c,top}$ as previously considered, the efficiency of the cell under 10% sun increases continuously and at a steeper rate. This continuous efficiency increase is also observed when augmenting the RJ's sheet resistance (Figure 12 (right)). This suggests that having high transverse and lateral resistances of the RJ will not degrade the cell when the illumination is reduced. Rather, this will ameliorate the cell performance. The behaviour of the PCE shown in Figure 12 (left) therefore indicates that a contact resistance limited by thermionic emission between the RJ and the shunted sub-cell would be a great advantage; at higher temperatures, resulting from high illumination, $R_{c,top}$ would be small but still sufficient to quench the shunts. At lower temperatures (low illumination), $R_{c,top}$ is bigger, which is required to quench the current leaks under these conditions.

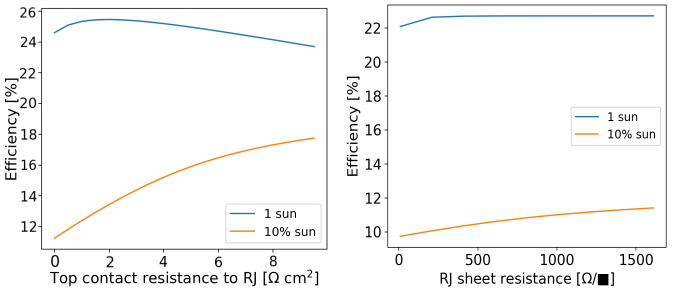

Fig. 12 Comparison between 1 sun or 10% sun light intensity on the efficiency of a 0.4% top shunted cell when varying the contact resistance between the RJ and the top cell (left) and of a 1% top shunted cell when varying the RJ's sheet resistance (right)

This sensitivity analysis shows that under different illuminations, changing the resistive properties of the RJ to mitigate the effects of shunting will not have a substantially degrading effect on the cell performance. On the contrary, it could lead to a proportionally larger gain in efficiency as suggested by the results at low light intensity. The overall effect of these observations on the yield of a solar cell could be calculated by incorporating meteorological data.[29,30] This would take into account real world spectral and intensity variations. However, this is beyond the scope of this study.

Another effect to be considered is the temperature of the cell. The measurements and simulations discussed here are for cells maintained at 25°C. However, cells in the field are subjected to important temperature variations. The short circuit current is negligibly affected by changes in temperature. This is less the case for the open circuit voltage where higher voltage solar cells are less affected by temperature. However, shunts have an important effect on reducing a cell's V_{oc}, meaning that these cells will be more affected by temperature increases. The contact resistance to the RJ's effect on increasing the Voc is therefore of great importance in commercial cells as it will reduce the efficiency loss due to temperature. This could be further investigated by obtaining the equivalent circuit parameters of cell's whose LIV curves were obtained at differ-

ent temperatures. https://www.pveducation.org/pvcdrom/solar-cell-operation/effect-of-temperature

4 Conclusions

As even small degrees of ohmic shunting on the baseline parameters can have severe effects on the efficiency of tandem cells, it is important to understand the dynamics of these defects in Pk/Si tandem solar cells. By modelling these cells with a circuit equivalent model, it was possible to examine the effect of varying the resistive properties of the recombination junction on the cell performance. It has been found that by optimising the contact resistance between the RJ and the shunted sub-cell, the leakage currents can be partially quenched leading to an increase in the cell performance greater than the losses relative to the increased series resistance. These results confirm that the approach of Despeisse *et al.* can also be applied to perovskite-based tandem solar cells. When the sheet resistance of the RJ is increased, the efficiency rises and saturates as the elements becomes completely isolated. However, the extent of the possible gain in efficiency is highly dependant on the severity of the shunt and the cell properties; high series and contact resistances in the shunted sub-cell tend to hinder the mitigating effect of the RJ's resistive properties on the performance loss due to shunting.

A sensitivity analysis was carried out to determine the potential of this effect under low illumination. It showed that although changing the current matching to a device limited by the shunted sub-cell reduced the cell performance, this amounts to less that 1% absolute efficiency. Furthermore, increasing the resistivity of the RJ at 10% sun leads to increasing PCEs over the considered resistance ranges. This shows that this approach is still valid under different illuminations, and perhaps even more importantly, at lower illuminations, the implications of which may have an important impact on the overall yield of a perovskite tandem solar cell. Depending on the eventual manufacturing yield of such devices, the work presented herein may have powerful consequences on improving the real world performance of these novel devices.

Further work should be carried out to determine the effect of different types of shunts in the absorber, ETL or HTL on the cell performance and whether some materials used for the shunted layers have innately high contact resistances between each other. Additionally, measurements could be carried out to experimentally determine the values of the contact resistances to the recombination junction. This would allow to have a circuit equivalent model that better describes reality and could potentially yield results that can be implemented in future cell architectures.

Conflicts of interest

There are no conflicts of interest to declare.

Acknowledgements

The authors would like to warmly thank Dr. Derk Batzner for his feedback on this work. This work was financed under the SNF Bridge project POWER (20B2-1_176552).

Notes and references

1 *Best Research-Cell Efficiency Chart*, 2020, https://www.nrel.gov/pv/cell-efficiency.html.
2 S. Ruhle, *Solar Energy*, 2016, **130**, 139–147.
3 A. Richter, M. Hermle and S. W. Glunz, *IEEE Journal of Photovoltaics*, 2013, **3**, 1184–1191.
4 F. I. for Solar Energy Systems ISE with support of PSE Projects GmbH, *Photovoltaics Report*, 2020, https://www.ise.fraunhofer.de/content/dam/ise/de/documents/publications/studies/Photovoltaics-Report.pdf.
5 L. A. Zafoschnig, S. Nold and J. C. Goldschmidt, *IEEE Journal of Photovoltaics*, 2020, **10**, 1632–1641.
6 W. Shockley and H. J. Queisser, *Journal of Applied Physics*, 1961, **32**, 510–519.
7 A. D. Vos, *Journal of Physics D: Applied Physics*, 1980, **13**, 839–846.
8 C. Feser, J. Lacombe, K. v. Maydell and C. Agert, *Progress in Photovoltaics*, 2011, **20**, 74–81.
9 J. P. Connolly, D. Mencaraglia, C. Renard and D. Bouchier, *Progress in Photovoltaics*, 2014, **22**, 810–820.
10 S. D. Wolf, J. Holovsky, S.-J. Moon, P. Loper, B. Niesen, M. Ledinsky, F.-J. Haug, J.-H. Yum and C. Ballif, *The Journal of Physical Chemistry Letters*, 2014, **5**, 1035–1039.
11 M. A. Green, A. Ho-Baillie and H. J. Snaith, *Nature Photonics*, 2014, **8**, 506–514.
12 X. Wu, M. T. Trinh, D. Niesner, H. Zhu, Z. Norman, J. S. Owen, O. Yaffe, B. J. Kudisch and X.-Y. Zhu, *Journal of the American Chemical Society*, 2015, **137**, 2089–2096.
13 H. Oga, A. Saeki, Y. Ogomi, S. Hayase and S. Seki, *Journal of the American Chemical Society*, 2014, **136**, 13818–13825.
14 S. D. Stranks and H. J. Snaith, *Nature Nanotechnology*, 2015, **10**, 391–402.
15 Z. Song, C. Chen, C. Li, R. A. Awni, D. Zhao and Y. Yan, *Semiconductor Science and Technology*, 2019, **34**, 093001.
16 A. Al-Ashouri, E. Köhnen, B. Li, A. Magomedov, H. Hempel, P. Caprioglio, J. A. Márquez, A. B. M. Vilches, E. Kasparavicius, J. A. Smith, N. Phung, D. Menzel, M. Grischek, L. Kegelmann, D. Skroblin, C. Gollwitzer, T. Malinauskas, M. Jost, G. Matic, B. Rech, R. Schlatmann, M. Topic, L. Korte, A. Abate, B. Stannowski, D. Neher, M. Stolterfoht, T. Unold, V. Getautis and S. Albrecht, *Science*, 2020, **370**, 1300–1309.
17 M. H. Futscher and B. Ehrler, *ACS Energy Letters*, 2017, **2**, 2089–2095.
18 F. Wang, S. Bai, W. Tress, A. Hagfeldt and F. Gao, *npj Flexible Electronics*, 2018, **2**, 22.
19 S. Heo, G. Seo, Y. Lee, D. Lee, M. Seol, J. Lee, J.-B. Park, K. Kim, D.-J. Yun, Y. S. Kim, J. K. Shin, T. K. Ahn and M. K. Nazeeruddin, *Energy & Environmental Science*, 2017, **10**, 1128–1133.
20 L. Cai, L. Liang, J. Wu, B. Ding, L. Gao and B. Fan, *Journal of Semiconductors*, 2017, **38**, 014006.
21 I. Lombardero and C. Algora, *Solar Energy Materials and Solar Cells*, 2020, **204**, 110236.
22 M. Despeisse, M. Boccard, G. Bugnon, P. Cuony, T. Söder-

ström, G. Parascandolo, M. Stuckelberger, M. Charriere, L. Lofgren, C. Battaglia, S. Hänni, A. Billet, L. Ding, S. Nicolay, F. Meillaud, N. Wyrsch and C. Ballif, Low-conductivity doped layers for improved performance of thin film silicon solar cells on highly textured substrates, 2010.

23 U. Rau, P. O. Grabitz and J. H. Werner, *Applied Physics Letters*, 2004, **85**, 6010.

24 F. Oviedo, Z. Liu, Z. Ren, M. Thway, T. Buonassisi and I. M. Peters, *Japanese Journal of Applied Physics*, 2017, **56**, 08MA05.

25 M. Boccard and C. Ballif, *ACS Energy Letters*, 2020, **5**, 1077–1082.

26 S. M. Sze and K. K. Ng, *Physics of Semiconductor Devices*, John Wiley and Sons, Inc., Hoboken, New Jersey, 3rd edn, 2007.

27 N. Mundhaas, Z. J. Yu, K. A. Bush, H. Wang, J. Hausele, S. Kavadiya, M. D. McGehee and Z. C. Holman, *Solar RRL*, 2019, **3**, 1800378.

28 J. Haschke, R. Lemerle, B. Aissa, A. A. Abdallah, M. M. Kivambe, M. Boccard and C. Ballif, *IEEE Journal of Photovoltaics*, 2019, **9**, 1202–1207.

29 O. Dupre, B. Niesen, S. D. Wolf and C. Ballif, *The Journal of Physical Chemistry Letters*, 2018, **9**, 446–458.

30 M. T. Horantner and H. J. Snaith, *Energy & Environmental Science*, 2017, **10**, 1983–1993.